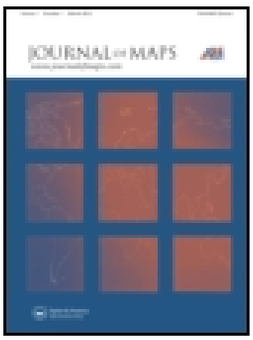

Journal of Maps

ISSN: (Print) (Online) Journal homepage: https://www.tandfonline.com/loi/tjom20

# Multi-temporal UAV based repeat monitoring of rivers sensitive to flood

Orkan Özcan & Okan Özcan

**To cite this article:** Orkan Özcan & Okan Özcan (2020): Multi-temporal UAV based repeat monitoring of rivers sensitive to flood, Journal of Maps, DOI: 10.1080/17445647.2020.1820387

**To link to this article:** https://doi.org/10.1080/17445647.2020.1820387

JOURNAL OF MAPS
https://doi.org/10.1080/17445647.2020.1820387



# Multi-temporal UAV based repeat monitoring of rivers sensitive to flood

Orkan Özcan [a] and Okan Özcan [b]

[a]Eurasia Institute of Earth Sciences, Istanbul Technical University, Istanbul, Turkey; [b]Department of Civil Engineering, Akdeniz University, Antalya, Turkey

**ABSTRACT**

Multi-temporal repeat monitoring of flood-vulnerable rivers is crucial due to rapid alteration of morphological properties of in-channel landforms. Besides, the characteristics of the river crossing bridges may deteriorate due to flood induced scouring around bridge piles or due to flood loads. Thus, in this study high-resolution topography of the study region was acquired during two consecutive years by unmanned aerial vehicle (UAV) based surveys using Structure-from-Motion (SfM) processing. Following the extraction of digital elevation models (DEM), repeat data that were obtained at each UAV survey were compared using Geomorphic Change Detection (GCD) to calculate volumes of deposition and erosion via DEM of difference (DoD) algorithm. Thus, detailed high-resolution maps of the river channels can be rapidly and efficiently generated by low cost UAV based measurement methods in order for continuous tracking of stream channel morphology for the rivers sensitive to floods.

**ARTICLE HISTORY**
Received 1 July 2020
Revised 18 August 2020
Accepted 3 September 2020

**KEYWORDS**
Flood; UAV; bridge; scour; change detection; dem of difference

## 1. Introduction

River topography measurement is a major concern of fluvial geomorphology since topography is the most basic descriptor pertinent to geomorphology and geomorphic process (Woodget et al., 2014). For the hydrologic applications with high spatial resolution, proper scaling should be considered due to the increment of data both in space and time. Herein, unmanned aerial vehicles (UAVs) provide an effective solution to this issue that depend on scale in hydrologic applications while supplying imaging and sensing equipment mounted on the platforms which constitute an unmanned aerial system (UAS) (Dyer et al., 2020; Ozcan & Ozcan, 2019; Rusnák et al., 2018; Tamminga et al., 2015; Woodget et al., 2014). Since the UAV based measurement methods procure data at extremely high spatial resolution (centimeter scale), the measurement precision is comparable to traditional surveying techniques (Carrera-Hernández et al., 2020). The direct applications of UAV-based measurement methods related to elevation, aspect, and stream distribution was useful in surface investigations and in analyzing hydrologic response by means of river mapping and floodplain characterization (Rusnák et al., 2018), riverbank and floodplain surveying (Tamminga et al., 2015), scour monitoring in bridges (Ozcan & Ozcan, 2018; Ozcan & Ozcan, 2019), and DEM generation over various scales and landscapes (Gafurov, 2018). UAV-based measurements provide a data collection platform between the point (i.e. terrestrial measurements) and regional scale (i.e. spaceborne measurements) with a spatial extent and resolution (Pajares, 2015). Thus, UAVs can be used for rapid and low-cost monitoring of surface characteristics, features, and processes in hydrologic and geomorphological applications such as large-scale mapping of flood plains or river basins, especially for the regions with limited or no access.

Regarding three-dimensional (3D) dense point cloud generation by Structure from Motion (SfM) technique via UAV derived images, the accuracy was demonstrated to be comparable to traditional high-resolution topographical survey methods for the regions having different geomorphic properties (Javernick et al., 2014; Ozcan, 2019). This technique is shown as reliable and efficient for collecting surface data for streams and rivers (Micheletti et al., 2015). For river bathymetry modeling, the bathymetric data acquired from high-resolution UAV-derived images at shallow water were verified with real data and high correlation was obtained (Flener, 2013; Ozcan & Ozcan, 2018, 2019).

Geomorphic change detection (GCD) analysis method was implemented with the DEM of Difference (DoD) algorithm in order to estimate quantitative landform alterations, in various environments (Hicks, 2012; Wheaton et al., 2010). The geomorphic changes can be determined by in-channel landform change monitoring (Clapuyt et al., 2016; Cook, 2017; Javernick et al., 2014) and by morphometric measurements (Gómez-Heras et al., 2019) via UAS technologies. Further, the implementation of high-resolution

CONTACT Orkan Özcan ozcanork@itu.edu.tr Eurasia Institute of Earth Sciences, Istanbul Technical University, Istanbul 34469, Turkey
Supplemental data for this article can be accessed at https://doi.org/10.1080/17445647.2020.1820387

topographic survey methods (Vericat et al., 2017) induced spatial investigation of topographic changes at multiple temporal and spatial scales. Hereby, despite the reliable quantification of landform change rates, the magnitude of the changes relating the main geomorphic processes, morphometric characteristics, and spatial and temporal distribution was not quantified (Llena et al., 2020). The alterations in geomorphic features can be quantified via two DEM data sets that were obtained for two different periods. The estimated amounts of erosion and deposition in a vast area should be verified through field measurements. Thus, in this study, in-channel morphological changes of a flood-vulnerable river in Bogacay plain were evaluated by UAV based repeat monitoring via DoD algorithm.

## 2. The study region

Bogacay plain of lagoon origin, which is located southwest of the city of Antalya, Turkey is the subject of this study (Figure 1). Antalya is located at the southern margin of the Western Tauride Belt and the region includes platform-type carbonate sediments that were deposited between the Late Cambrian and Eocene. Bey mountains comprise platform-type carbonate sediments of Jurassic to Miocene age (Akay et al., 1985). The Bogacay Plain evolved during the Quaternary concerning eustatic sea-level changes and tectonic activity by which bays in the west of Antalya was comprised. In the region, river-bed and other fluvial deposits include coarse gravels and medium to fine sands for which the material sources were Cretaceous limestone and ophiolitic mélange (Dipova, 2020).

Since the TanDEM-X (DLR, 2016) having 12.5 m resolution has shown to have the highest effective topographic detail compared to other DEMs (i.e. SRTM, ASTER, AW3D) (Boulton & Stokes, 2018), Red Relief Image Map (RRIM) (Chiba et al., 2008) (Figure 1a), derived from the TanDEM-X was used as the base map to extract the watershed. The Bogacay basin is located at the western region of Antalya city center with a watershed of about 4072 km$^2$ (Figure 1a). Agricultural areas and villages in Bogacay plain have been plagued by flooding in the past due to instantaneous precipitation and high slope behind the plain (Figure 1b). In the Bogacay basin, approximately 14% of the watershed is above 1500 m altitude which increases to 2000 m for an extent of 27 km away from the sea. Herein, the slopes along the Guver and Candir branches are higher than that of the other branches (Doyran and Karaman branches) as shown in the profiles given with the slopes ranging from 0.1% to 2.0% (Figure 1b). In Antalya city center, 54% of annual average precipitation of approximately 1200 mm

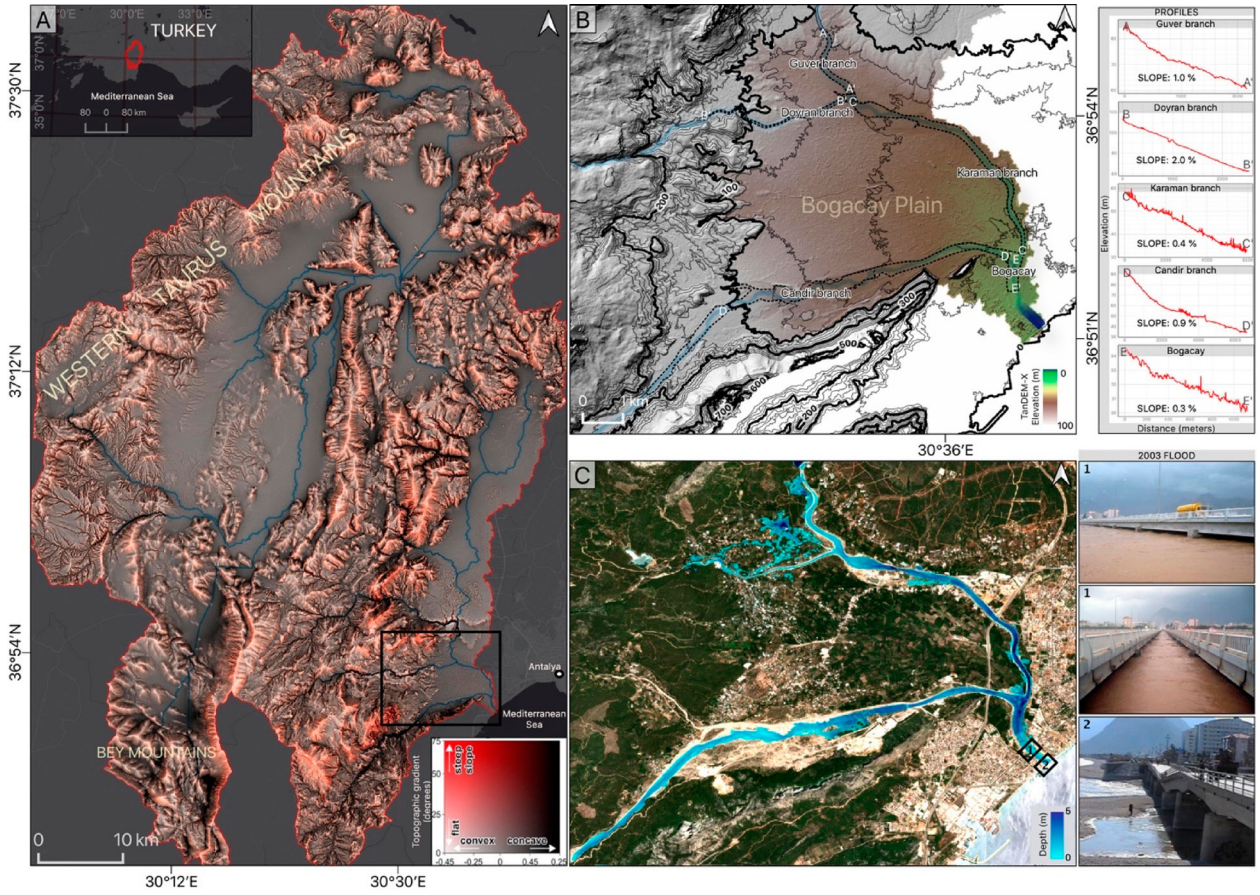


**Figure 1.** (a) RRIM of Bogacay watershed, study region (b) floodplain with branch profiles, and (c) previously obtained flood hazard map showing bridge water level and damaged bridge due to the flood occurred in 2003 (Ozcan & Ozcan, 2020).

occurs in winter season. The peak discharge rate and relevant sediment volume is reached in January and February however, discharge and sediment flow continuously reduce between March and August, and negligible rates are observed between September and November (Oğuz, 2001).

Further, the highway bridge located at Bogacay estuary was heavily damaged due to flood induced scour in bridge substructure during the December 2003 flood that corresponded to a 50-year return period with a measured discharge of 1940 $m^3/s$, while all of the 260 m wide river channel was observed to be filled with sediments (DSHW, 2018). The water level was observed to reach the girder level for the nearby bridge located at the north and water was observed to partly overflow the river channel while inundating the zoning areas. Herein, UAV generated point clouds were used to obtain the river DEMs via SfM algorithm and relevant hydraulic analyses were conducted based on flood/scouring by using the HEC-RAS software and the multi-hazard bridge performance under flood and seismic loads was previously evaluated (Ozcan & Ozcan, 2020) (Figure 1c). Preliminary results verified the significant impact of flood on bridge performance in 2003 that induced substantial amount of scour around bridge piles. Besides, seasonal hydrogeomorphological changes between 2016 and 2018 in the Bogacay estuary have been evaluated by using high-resolution UAV-derived orthophotos and DEMs, as well (Ozcan & Ozcan, 2019). The landform changes were determined to have the utmost influence on the multi-hazard performance of the bridges at the study region. Since the lagoon part of the Bogacay recreation project started to retain water in September 2018, the Bogacay estuary region was not considered in this study.

## 3. Methods

### 3.1. Stream and watershed generation

The implemented watershed extraction method includes three steps following the preprocessing of DEM and the definition of stream flow steps namely generation of accumulated grids, stream network, and watershed boundaries. Arc Hydro Tools were used in order to acquire watershed features and delineated watersheds (Maidment, 2002). The Bogacay basin boundary was extracted from TanDEM-X digital elevation data as mentioned above (Figure 1a). Herein, the flow network was identified by flow directions and the flow accumulation regions. The basin boundaries were attained by revealing the sub basin boundaries and the adjoint basins.

### 3.2. UAV surveys and data processing

In this study two field surveys were conducted on July 2018 and May 2019 which were compared with one another to identify changes in the stream channel from one year to the next. The DEMs of the river basin was acquired by a UAV via 152 GCPs taken along the river region (Figure 2). Aerial photographs were collected using DJI Mavic Platinum Pro equipped with a 12 MP camera mounted on a

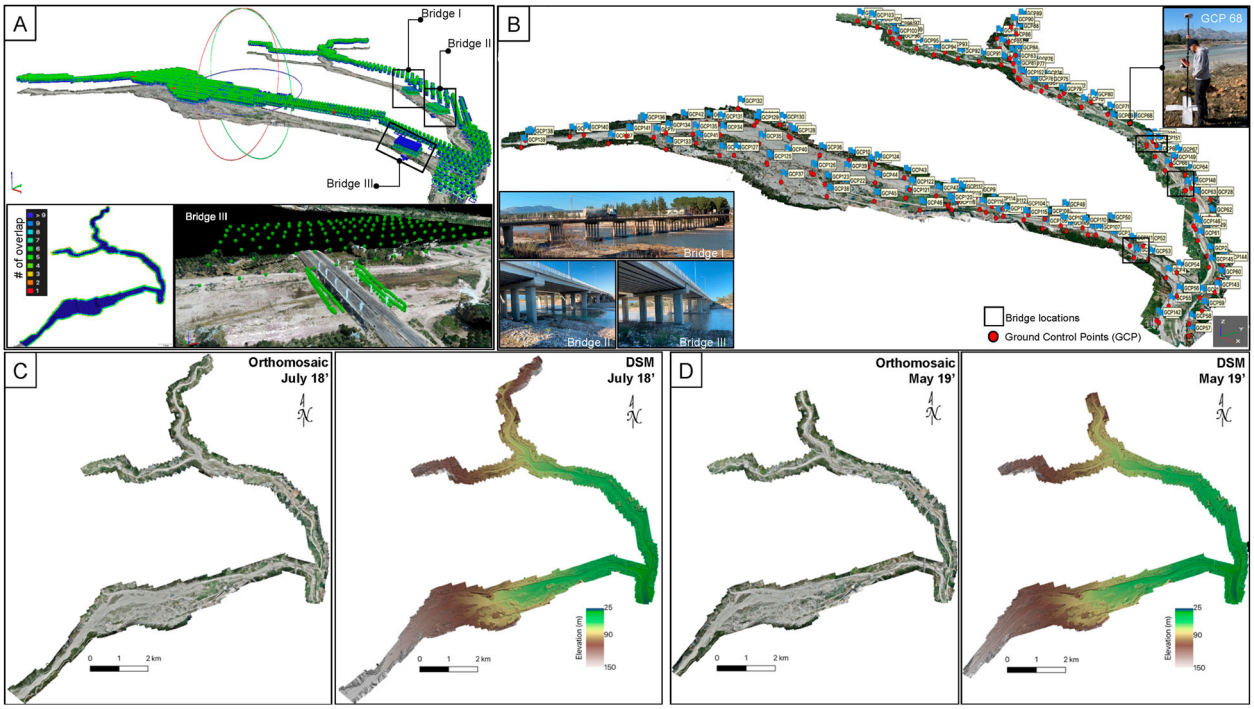


**Figure 2.** (a) UAV survey flight plan with bridge locations, (b) GCP locations on a dense point cloud, and orthomosaics with DSMs for (c) July 2018 and (d) May 2019.

stabilized gimbal and internal GPS. While covering a stream channel area of approximately 18 km$^2$ during the flights, 1969 and 1696 images were collected at an average altitude of 330 m in July 2018 and in May 2019, respectively (Figure 2a). Prior to each flight, GCPs were laid out in the study area along the banklines and inside the river channel to ensure proper geolocation of the SfM model. GCP sets were surveyed with an RTK enabled Leica GS09 GPS where data quality (3D quality, i.e. horizontal and vertical) was 0.020 m on average (Figure 2b). In model generation, following the camera alignment and referencing processes, the accuracy of the generated point cloud was evaluated. Moreover, the nonvisual DEM regions that were located below bridge decks were derived by manual designation of the flight heights with varying camera angles (i.e. inset in Figure 2a,b). Thus, the overlapping ratios for aerial images were optimized as 85% both in direction of motion and in lateral direction. For bridge modeling, approximately 150 images were acquired for each bridge and ground sampling distance (GSD) was obtained as 1–2 cm/pixel while satisfying high spatial resolution. Each bridge was processed separately and then merged with the entire model using appropriate manual tie points.

In data processing after each UAV survey, SfM photogrammetry was implemented using standard workflow of Agisoft Metashape Professional 1.6. Herein, concerning the simultaneous solution of model geometry, position and orientation data, the relation between the images, the sensed features were monitored between the images. Then, the 3D location of the object was estimated by feature trajectories and camera movement (Javernick et al., 2014). Initial SfM processing resulted in a sparse point cloud with 1348800 and 1228006 points for July 2018 and May 2019, respectively. The high-resolution dense point clouds were created with mild filtering that resulted in a model with approximately 690 and 600 million points for July 2018 and May 2019 surveys, respectively. Point clouds were filtered to remove outliers and vegetation manually. Meanwhile, the orthomosaics and DEMs were generated for July 2018 and May 2019 for geomorphic detection analysis (Figure 2c,d).

Dense point clouds with an average point density of approximately 24 points/m$^2$ was obtained for both surveys while registering SfM datasets by the GCP network. According to the Agisoft processing report, GSD was acquired with an average of 10.2 cm/pixel for both surveys. The validation metrics that were used to analyze the quality differences were the mean error (ME) as a measure of the accuracy and the standard deviation of the elevations (SDE) as a measure of the precision (Equations (1) and (2)). Herein, $n$, $z_{\mathrm{mod}}$, $z_{\mathrm{obs}}$ denote the number of points, DEM elevations, and height of GCPs measured with RTK, respectively.

$$\mathrm{ME} = \frac{\sum_i^n (z_{\mathrm{mod}} - z_{\mathrm{obs}})}{n} \tag{1}$$

$$\mathrm{SDE} = \sqrt{\frac{\sum_i^n ((z_{\mathrm{mod}} - z_{\mathrm{obs}}) - ME)^2}{n-1}} \tag{2}$$

$$\mathrm{RMSE} = \sqrt{\frac{\sum_i^n (z_{\mathrm{mod}} - z_{\mathrm{obs}})^2}{n}} \tag{3}$$

For the measurements in July 2018, GCP total accuracies were obtained as 10.8, 10.5 and 28.7 cm with a total root mean square error (RMSE, Equation (3)) of 31.3 cm in the $x$, $y$ and $z$ directions, respectively. However, for May 2019, GCP accuracies were calculated as 11.2, 10.1 and 27.3 cm with a total RMSE of 30.6 cm in the $x$, $y$ and $z$ directions respectively. For bridge modeling, the accuracy of UAV-derived orthomosaics was found not to exceed 0.055 and 0.082 m in the horizontal and vertical, respectively.

### 3.3. Bridge deck removal

In order to procure more spatial detailing of the river bed bathymetry under the bridges and to fully represent the basin area in the DEMs, point clouds were filtered by manually removing the points inside the point clouds for the decks of each bridge (Figure 3).

In order to generate the main map, UAV-derived DEM at 20-centimeter resolution (i.e. cell size) and TanDEM-X with a 12.5-meter resolution were combined. The higher resolution data at the river bed (UAV-derived DEM) and the lower resolution data for the remaining watershed (TanDEM-X) were fused with the given expression in Equation (4) which was applied with ArcGIS 10.3 raster calculator. Consequently, the UAV derived surface models were combined with resampled TanDEM-X digital surface model which may be used in detailed hydraulic modeling.

$$\begin{aligned}&\mathrm{Con}(\mathrm{IsNull}(``\mathrm{UAV} - \mathrm{derivedDEM}\}),\\ &``\mathrm{resamapledTanDEM} - \mathrm{X}\},\ ``\mathrm{UAV} - \mathrm{DEM}\})\end{aligned} \tag{4}$$

### 3.4. Geomorphic change detection

The volumetric calculations using DEMs were performed by tracking the height changes in the overlapping pixels for measurement intervals on the same surface. In order to compare the volumetric changes of the periodically obtained data, DoD method was used in which the volumetric variations between topographic surfaces were calculated on pixel-by-pixel basis regarding two different DEMs. This method is widely

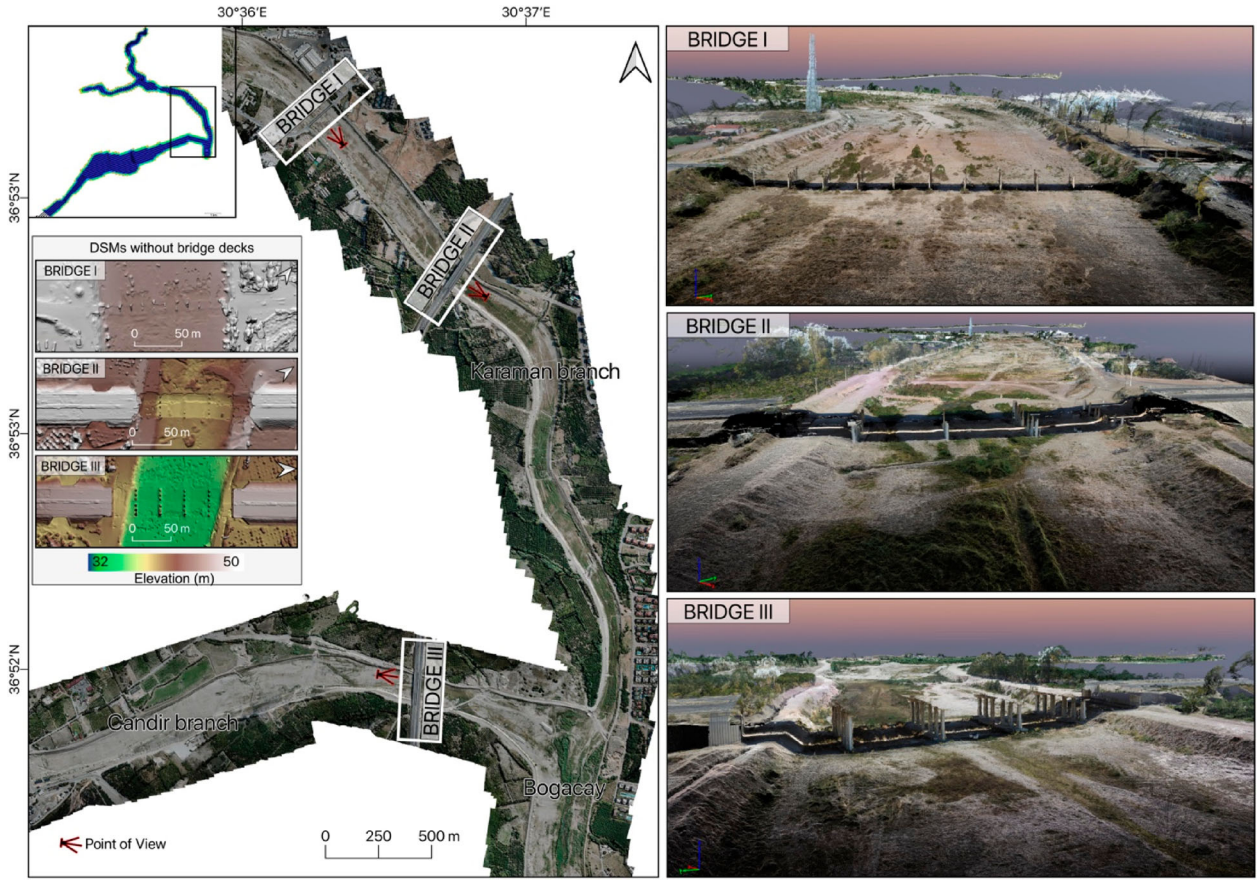


**Figure 3.** The bridge locations and the related point clouds only with bridge piers. Inset shows the DEMs with removed decks for the bridges I, II, and III.

used to monitor the sizes of geomorphological changes and spatial patterns such as tectonic movement, erosion, sediment transport and deposition (Williams, 2012). The GCD analysis incorporates DoD algorithm processed using Geomorphic Change Detection Tool – GCD v7.2 (Wheaton et al., 2010) to estimate the volumetric landform changes. The DoD algorithm computes the pixel value differences of two DEMs (Equation (5)), where $\delta_E$ is the output DEM indicating volumetric changes ($m^3$); $Z_1$ is the DEM of earlier period (i.e. UAV-derived DEM acquired on July 2018), and $Z_2$ is the DEM of later period (i.e. UAV-derived DEM acquired on May 2019). Herein, negative values indicate surface lowering or erosion, and positive values indicate surface raising or deposition. Minimum level of detection ($LoD_{min}$) threshold was used as 0.20 m in order to distinguish the natural noise occurring on the surface, which must be detected while identifying surface alterations. In the study region, since both field surveys were conducted in the summer time when the surface runoff was minimum, the channel bed was considered as dry. Thus, the water induced errors (i.e. refraction) were neglected during DoD processing.

$$\delta_E = Z_2 - Z_1 \quad (5)$$

## 4. Topographic changes

The DoD results obtained for the Bogacay Plain were given in Figure 4a and close-up views for the selected regions on the Candir branch, Doyran branch, and Bogacay are presented in Figure 4b–d, respectively. Herein, change maps on TanDEM-X hillshade were given at each selected region with the detailed RRIM maps obtained on July 2018 and May 2019. Surface lowering was mainly located at the areas having relatively higher slopes (1.0–2.0%, Figure 1b) and at the main channels. Yet surface raising was mainly observed in the deposition zones that are located at the toe of the slopes near the main channels and in the main channels themselves, as well. In all maps, red indicates surface lowering (erosion) while blue represents surface raising (deposition) which were significant up to 1 meter of change in the river channel. For the region located on the Candir branch, the change map given in the Figure 4b indicates stream induced deposition on the lower course due to winter precipitation. Similar landform change pattern was observed for the region at Doyran branch, however bankline erosion was present in downstream (Figure 4c). In contrast, at the connection region of Karaman and Candir branches which forms Bogacay main

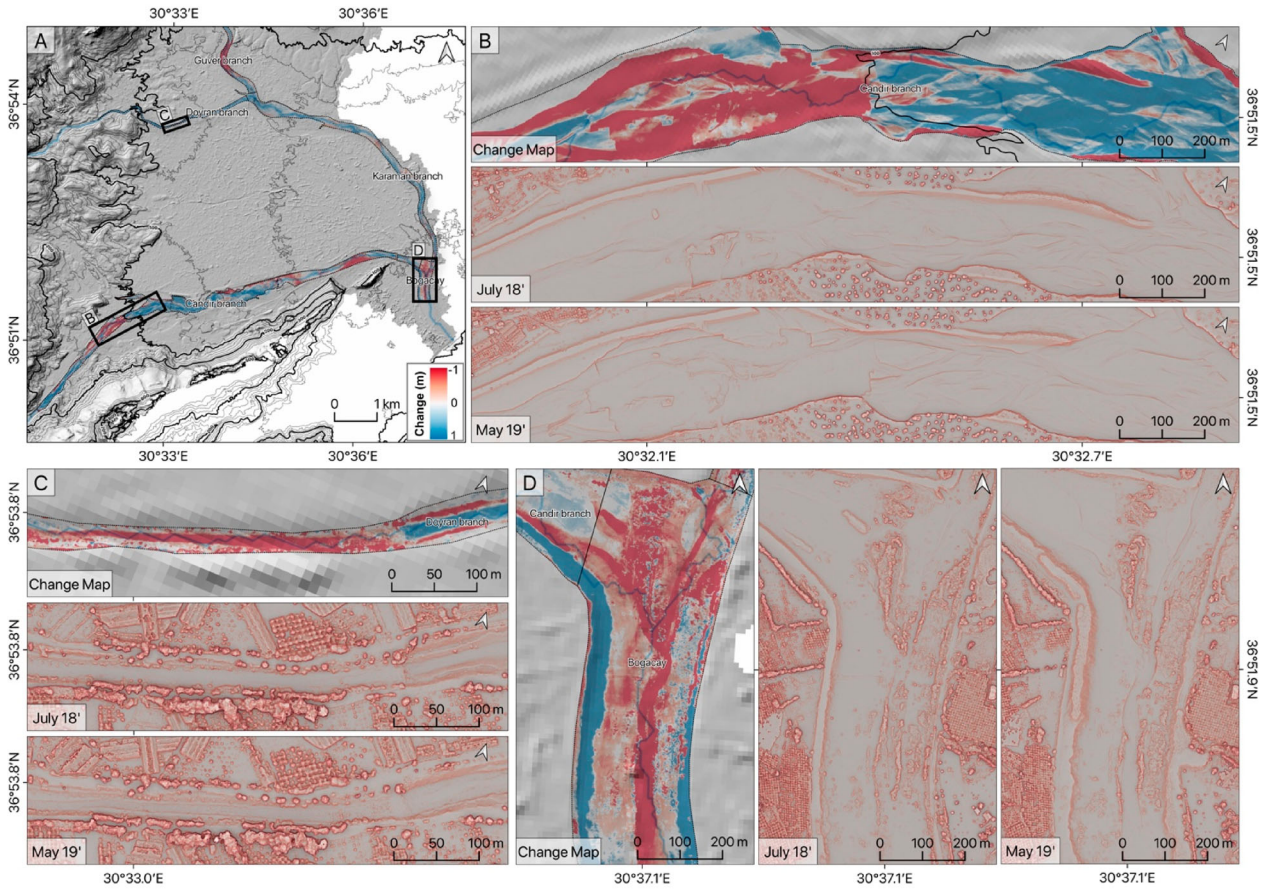


**Figure 4.** DoD results for the (a) selected regions on the branches of (b) Candir, (c) Guver, and (d) Bogacay.

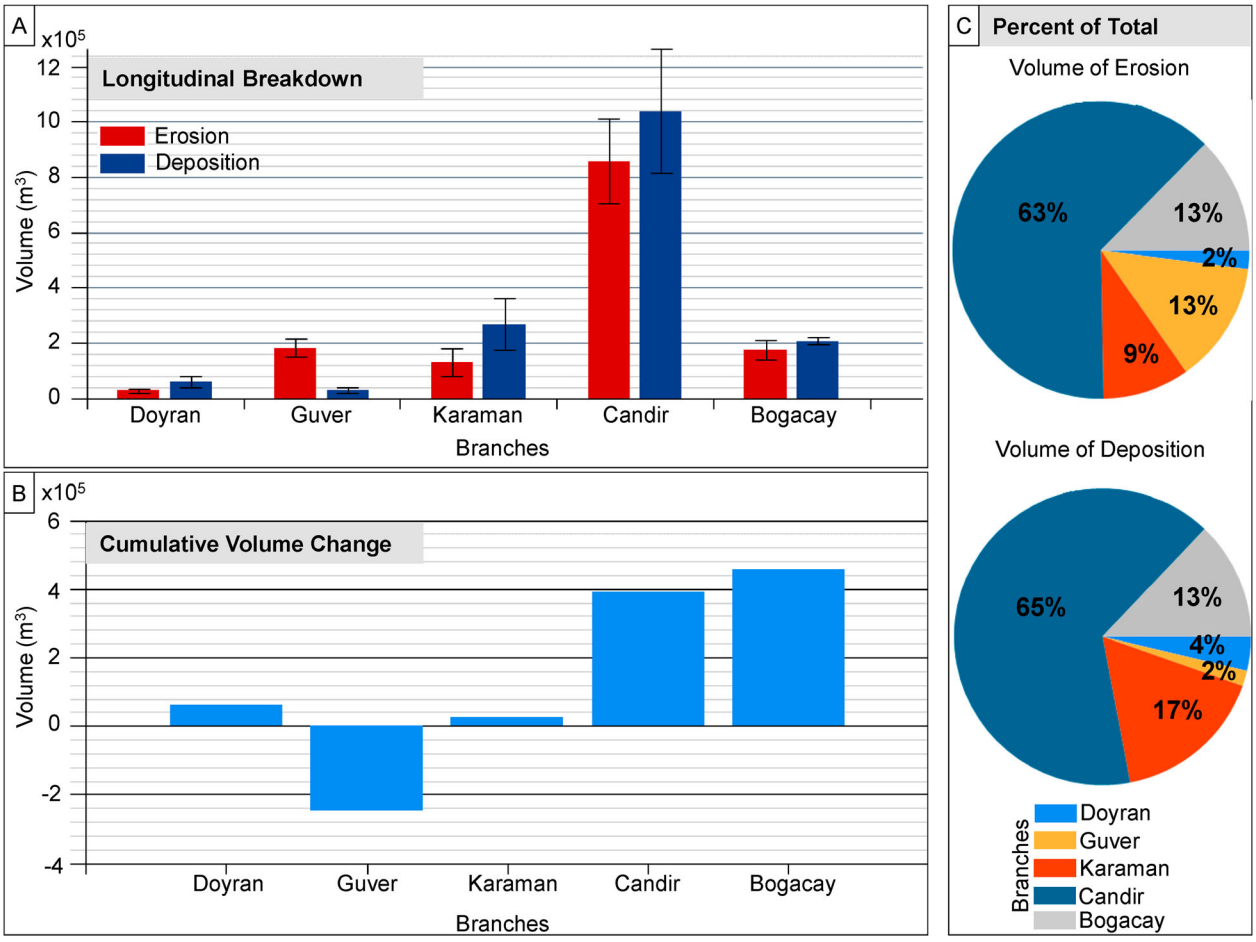


**Figure 5.** DoD quantification regarding (a) longitudinal breakdown, (b) cumulative volume change, and (c) total percentages.

channel the significant river bed erosion was observed for all branches. The bankline deposition at Bogacay indicates that the amount of sediments transported from Candir branch was more pronounced compared to other.

### 4.1. Quantification of morphological changes

As a result of GCD analysis, the amounts of eroded and deposited materials were quantified for all branches both separately (Figure 5a) and cumulatively (Figure 5b). Accordingly, the total percentage of volumetric changes in the flood plain are given in Figure 5c concerning all branches. Regarding the longitudinal breakdown of the landform changes (Figure 5a), the Candir branch has maximum volume of erosion and deposition with the highest standard deviation among others as shown in the box plots. As expected, erosion exceeds deposition where the slope is steep (i.e Guver branch), however in the other branches except Doyran, the higher amount of deposition exists due to lower slope. Likewise, the cumulative volume change graph (Figure 5b), which indicates the difference between the eroded and deposited materials, showed that Guver and Candir branches have the maximum eroded and deposited volumes, respectively. As shown in Figure 5c, Candir branch was observed to carry approximately 65% of the entire sediments throughout the floodplain. The other branches could reach at most 17% at Karaman branch concerning the deposited sediment volume (Figure 5c).

## 5. Discussion and conclusion

Accurate extraction of high-resolution DEMs are critical for many flood sensitive rivers regarding landform change monitoring (i.e. erosion and deposition), hydraulic modeling, sediment transport tracking, and evaluation of river channel morphodynamics. Thus, repeated high-resolution topography of the Bogacay basin, Antalya, Turkey was obtained in this study by means of UAV based SfM photogrammetry which was used to monitor topographic changes across multiple temporal scales. The acquired topography during two consecutive years allows analysis of the relations between the main geomorphic processes related to landform alterations and their role in sediment transfer. The results indicated that the alterations in the river channel by means of erosion and deposition after an expected flood event, allowed reliable evaluation of riverbed morphodynamics, while verifying that UAV SfM and DoD are useful tools in geomorphological dynamic mapping and in change monitoring studies. Further, future studies can be conducted on UAV-mounted bathymetric Lidar solutions to overcome the limitations of image-based measurements in underwater regions.

## Software

RRIM was produced with SAGA GIS. Hydrologic information extracted by using ESRI ArcGIS AddIn-ArcHydro. UAV data were processed using Agisoft Metashape Professional V1.6. Topographic changes were calculated by DoD algorithm based GCD analysis using ESRI ArcGIS AddIn-Geomorphic Change Detection Tool GCD v7.2. The main map was prepared by using Quantum GIS v 3.12.

## Acknowledgments

This study was supported by the Istanbul Technical University Scientific Research Project (ITU-BAP) [grant number MGA-2018-41393] and Akdeniz University Scientific Research Project (AU-BAP) [grant number FBA-2018-2877].

## Disclosure statement

No potential conflict of interest was reported by the author (s).

## Funding

This study was supported by research fund of Istanbul Technical University [grant number: MGA-2018-41393] and by research fund of Akdeniz University [grant number FBA-2018-2877].

## ORCID

*Orkan Özcan* http://orcid.org/0000-0002-7485-6157
*Okan Özcan* http://orcid.org/0000-0001-9905-1657

## References

Akay, E., Uysal, Ş, Poisson, A., Cravatte, J., & Müller, C. (1985). Antalya Neojen havzasının stratigrafisi. *Türkiye Jeoloji Kurultayi Bülteni*, *28*(2), 105–121. Ankara (in Turkish).

Boulton, S. J., & Stokes, M. (2018). Which DEM is best for analyzing fluvial landscape development in mountainous terrains? *Geomorphology*, *310*, 168–187. https://doi.org/10.1016/j.geomorph.2018.03.002

Carrera-Hernández, J. J., Levresse, G., & Lacan, P. (2020). Is UAV-SfM surveying ready to replace traditional surveying techniques? *International Journal of Remote Sensing*, *41* (12), 4818–4835. https://doi.org/10.1080/01431161.2020.1727049

Chiba, T., Kaneta, S.-I., & Suzuki, Y. (2008). Red relief image map: New visualization method for three-dimensional data. *The International Archives of the Photogrammetry, Remote Sensing and Spatial Information Sciences*, *37* (B2), 1071–1076. https://doi.org/10.11212/jjca1963.45.27

Clapuyt, F., Vanacker, V., & Van Oost, K. (2016). Reproducibility of UAV-based earth topography reconstructions based on structure-from-motion algorithms. *Geomorphology*, *260*, 4–15. https://doi.org/10.1016/j.geomorph.2015.05.011

Cook, K. L. (2017). An evaluation of the effectiveness of low-cost UAVs and structure from motion for geomorphic

change detection. *Geomorphology*, *278*, 195–208. https://doi.org/10.1016/j.geomorph.2016.11.009

Dipova, N. (2020). Investigation of relationship between Boğaçay (antalya) sediment transport and Konyaalti coastline via image processing techniques. *International Journal of Engineering, Design and Technology*, *2*(1), 010–023.

DLR. (2016). TanDEM-X ground segment DEM products specification document TD-GS-PS-0021 v.3.1. DLR. (46 pp).

DSHW. (2018). *General directorate of state hydraulic works, water chamber of geological enginners* (Bogacay Project Evaluation Report). Antalya, Turkey, pp. 112. (in Turkish).

Dyer, J. L., Moorhead, R. J., & Hathcock, L. (2020). Identification and analysis of microscale hydrologic flood impacts using unmanned aerial systems. *Remote Sensing*, *12*(10), 1549. https://doi.org/10.3390/rs12101549

Flener, C. (2013). Calibrating deep water radiance in shallow water: Adapting optical bathymetry modeling to shallow river environments. *Boreal Environmental Research*, *18*, 488–502.

Gafurov, A. M. (2018). Small catchments DEM creation using unmanned aerial vehicles. *IOP Conference Series: Earth and Environmental Science*, *107*, 012005. https://doi.org/10.1088/1755-1315/107/1/012005

Gómez-Heras, M., Ortega-Becerril, J., Garrote, J., Fort, R., & López-González, L. (2019). Morphometric measurements of bedrock rivers at different spatial scales and applications to geomorphologic heritage research. *Prog Earth Planet Sc*, *6*(1), 29. https://doi.org/10.1186/s40645-019-0275-0

Hicks, D. M. (2012). Remotely sensed topographic change in gravel riverbeds with flowing channels. In M. Church, P. Biron, & A. Roy (Eds.), *Gravel-bed rivers: Processes, tools, environments*. Wiley-Blackwell. https://doi.org/10.1002/9781119952497.ch23

Javernick, L., Brasington, J., & Caruso, B. (2014). Modeling the topography of shallow braided rivers using structure – from – motion photogrammetry. *Geomorphology*, *213*, 166–182. https://doi.org/10.1016/j.geomorph.2014.01.006

Llena, M., Smith, M. W., Wheaton, J. M., & Vericat, D. (2020). Geomorphic process signatures reshaping sub-humid Mediterranean badlands: 2. Application to 5-year dataset. *Earth Surface Processes and Landforms*, *45*(5), 1292–1310. https://doi.org/10.1002/esp.4822

Maidment, D. R. (2002). *Arc hydro: GIS for water resources [EB/OL]*. ESRI press.

Micheletti, N., Chandler, J. H., & Lane, S. N. (2015). Structure from motion (SfM) photogrammetry: British society for geomorphology geomorphological techniques, chap. 2, sec. 2.2.

Oğuz, H. (2001). Boğaçay Havzasında Yapılan Faaliyetler Sonucu Antalya Körfezine Taşınan Kirlilik Yüklerinin Tespitive Çözüm Önerileri, Yüksek Lisans Tezi, Akdeniz Üniversitesi Fen Bilimleri Enstitüsü Çevre Bilimleri ABD (in Turkish).

Ozcan, O. (2019). Performance evaluation of bridges under scour by UAS based measurements. *Journal of Polytechnic*, *22*(2), 385–391. https://doi.org/10.2339/politeknik.450288

Ozcan, O., & Ozcan, O. (2018). Multi-hazard assessment of RC bridges using unmanned aerial vehicle-based measurements. *Baltic Journal of Road and Bridge Engineering*, *13*(3), 192–208. https://doi.org/10.7250/bjrbe.2018-13.412

Ozcan, O., & Ozcan, O. (2019). Effect of hydrogeomorphological changes in flood plain on bridge multi-hazard performance. *Fresenius Environmental Bulletin*, *28*(2), 956–962.

Ozcan, O., & Ozcan, O. (2020). Unmanned aerial vehicle-based automated bridge multi-hazard assessment system. IGARSS 2020 (to be held in Sept. 2020).

Pajares, G. (2015). Overview and current status of remote sensing applications based on unmanned aerial vehicles (UAVs). *Photogrammetric Engineering & Remote Sensing*, *81*(4), 281–330. https://doi.org/10.14358/PERS.81.4.281

Rusnák, M., Sládek, J., Kidová, A., & Lehotský, M. (2018). Template for high-resolution river landscape mapping using UAV technology. *Measurement*, *115*, 139–151. https://doi.org/10.1016/j.measurement.2017.10.023

Tamminga, A. D., Eaton, B. C., & Hugenholtz, C. H. (2015). UAS-based remote sensing of fluvial change following an extreme flood event. *Earth Surface Processes and Landforms*, *40*(11), 1464–1476. https://doi.org/10.1002/esp.3728

Vericat, D., Wheaton, J., & Brasington, J. (2017). Revisiting the morphological approach: Opportunities and challenges with repeat high-resolution topography. In D. T. Tsutsumi & J. B. Laronne (Eds.), *Gravel-bed rivers: Processes and disasters* (pp. 121–158). Wiley.

Wheaton, J. M., Brasington, J., Darby, S. E., & Sear, D. A. (2010). Accounting for uncertainty in DEMs from repeat topographic surveys: Improved sediment budgets. *Earth Surface Processes Landforms*, *35*, 136–156. https://doi.org/10.1002/esp.1886

Williams, R. (2012). DEMs of difference. *Geomorphological Techniques*, *2*, 1–17.

Woodget, A. S., Carbonneau, P. E., Visser, F., & Maddock, I. P. (2014). Quantifying submerged fluvial topography using hyperspatial resolution UAS imagery and structure from motion photogrammetry. *Earth Surface Processes and Landforms*, *40*(1), 47–64. https://doi.org/10.1002/esp.3613